ACS APPLIED MATERIALS & INTERFACES

Research Article

www.acsami.org

Lipid-AuNPs@PDA Nanohybrid for MRI/CT Imaging and Photothermal Therapy of Hepatocellular Carcinoma

Yongyi Zeng,[†,‡,§] Da Zhang,[‡,§] Ming Wu,[‡,§] Ying Liu,[∥] Xiang Zhang,[†] Ling Li,[†,‡,§] Zheng Li,[∥] Xiao Han,[⊥] Xueyong Wei,[∥] and Xiaolong Liu*[,‡,§]

[†]Liver Disease Center, The First Affiliated Hospital of Fujian Medical University, Fuzhou 350005, P. R. China

[‡]The United Innovation of Mengchao Hepatobiliary Technology Key Laboratory of Fujian Province, Mengchao Hepatobiliary Hospital of Fujian Medical University, Fuzhou 350025, P. R. China

[§]The Liver Center of Fujian Province, Fujian Medical University, Fuzhou 350025, P. R. China

[∥]State Key Laboratory for Manufacturing System Engineering, School of Mechanical Engineering, Xi'an Jiaotong University, Xi'an 710049, P. R. China

[⊥]Biotechnology Research Institute, Chinese Academy of Agricultural Sciences, Beijing 100081, P. R. China

Supporting Information

ABSTRACT: Multifunctional theranostic nanoparticles represent an emerging agent with the potential to offer extremely sensitive diagnosis and targeted cancer therapy. Herein, we report the synthesis and characterization of a multifunctional theranostic agent (referred to as LA-LAPNHs) for targeted magnetic resonance imaging/computed X-ray tomography (MRI/CT) dual-mode imaging and photothermal therapy of hepatocellular carcinoma. The LA-LAPNHs were characterized as having a core−shell structure with the gold nanoparticles (AuNPs)@polydopamine (PDA) as the inner core, the indocyanine green (ICG), which is electrostatically absorbed onto the surface of PDA, as the photothermal therapeutic agent, and the lipids modified with gadolinium−1,4,7,10-tetraacetic acid and lactobionic acid (LA), which is self-assembled on the outer surface as the shell. The LA-LAPNHs could be selectively internalized into the hepatocellular cell line (HepG2 cells) but not into HeLa cells due to the specific recognition ability of LA to asialoglycoprotein receptor. Additionally, the dual-mode imaging ability of the LA-LAPNH aqueous solution was confirmed by enhanced MR and CT imaging showing a shorter T_1 relaxation time and a higher Hounsfield unit value, respectively. In addition, the LA-LAPNHs showed significant photothermal cytotoxicity against liver cancer cells with near-infrared irradiation due to their strong absorbance in the region between 700 and 850 nm. In summary, this study demonstrates that LA-LAPNHs may be a promising candidate for targeted MR/CT dual-mode imaging and photothermal therapy of hepatocellular carcinoma.

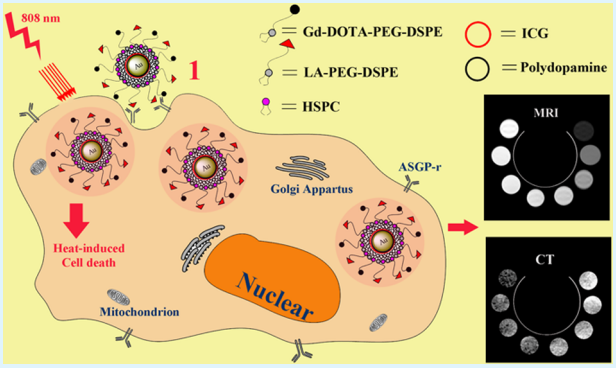

KEYWORDS: *AuNPs, polydopamine, lactobionic acid, dual-mode imaging, targeted photothermal therapy*

INTRODUCTION

Hepatocellular carcinoma (HCC) is one of the most lethal cancers worldwide and causes cancer-related death once distant malignancy has occurred.[1−6] Most patients are diagnosed at a late stage of the disease, resulting in poor prognosis. Early detection of lethal cancers, including HCC, remains challenging. Various imaging techniques, including computed X-ray tomography (CT),[7] magnetic resonance imaging (MRI),[8,9] ultrasound examination (US),[10] and positron emission tomography (PET),[11,12] have been extensively applied in clinical diagnosis of cancer. Among these imaging modalities, CT is one of the most convenient imaging/diagnostic tools in clinical application that provides three-dimensional structural details regarding tissues of interest based on various X-ray absorption features. However, CT suffers from low sensitivity for soft tissues because these tissues have low density.[13] In addition, iodinated compounds, which are clinically used as CT contrast agents, are limited by shot imaging time and potential renal toxicity due to rapid kidney clearance.[14] MRI, another powerful tool for whole-body diffusion-weighted imaging, is also extensively used in disease diagnosis, especially in soft tissues;[15] however, unenhanced MRI has the drawback of low-contrast sensitivity, which results in the poor distinction of a tumor from the surrounding tissue. Since either MRI or CT possesses its own characteristic strengths and weaknesses, the

Received: June 6, 2014
Accepted: August 4, 2014
Published: August 4, 2014

 © 2014 American Chemical Society

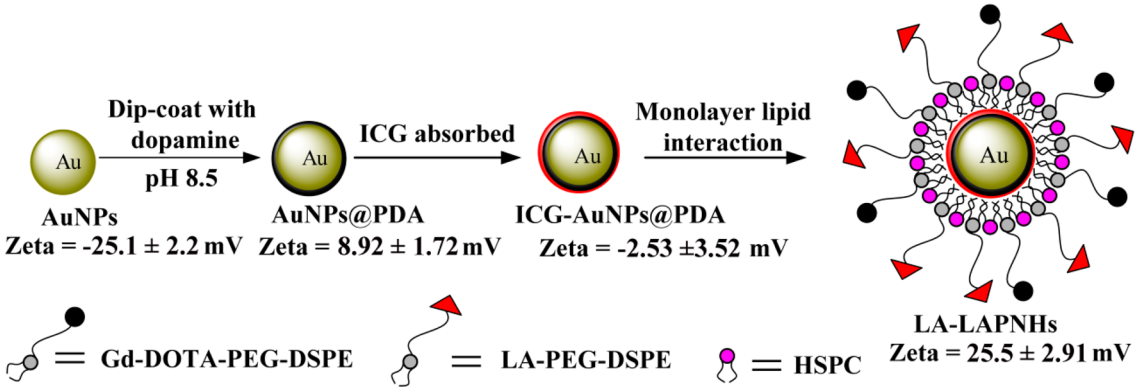

Figure 1. Schematic view of the LA-LAPNH preparation method. Indocyanine green (ICG) was electrostatically adsorbed onto the positively charged AuNPs@PDA to form ICG-AuNPs@PDA. Next, the lactobionic acid- and Gd(III)-DOTA-functionalized PEG-DSPE were self-assembled on ICG-AuNPs@PDA nanohybrids to construct the LA-LAPNHs.

combination of both imaging modalities may provide more comprehensive and accurate diagnostic information.

Advances in nanotechnology have provided opportunities for developing multimodal nanoprobes that can incorporate several contrast agents into a single system to improve contrast-enhanced imaging interpretation for the diagnosis of cancers. Theranostics, which combines the modalities of therapy and diagnostic imaging through the delivery of the therapeutic drugs and the diagnostic imaging agents in a single complex or at the same time, could significantly decrease the side effects of separated agents, facilitate the ablation of disease lesions in a well-controlled manner and at desirable locales, and overcome undesirable differences in biodistribution and selectivity that currently exist between imaging and therapeutic agents.[16,17] Although many research efforts have focused on developing nanomaterial-based CT/MR dual-mode contrast agents, such as gadolinium (Gd)-chelated gold nanoparticles (AuNPs),[18] biocompatible magnetite/gold nanohybrid contrast agents,[19] Gd-G_8dendrimers,[20] Fe_3O_4@P(St/MAA)@chitosan@Au core/shell NPs,[21] and polymer-stabilized lanthanide fluoride NPs,[22,23] it would be more attractive if the therapeutic and specific targeting ability could be further combined.[24−27]

Photothermal therapy (PTT) has been explored for the treatment of malignant carcinoma because of its high selectivity and minimal invasiveness.[28] Following near-infrared (NIR) laser irradiation, photosensitizing agents convert electromagnetic wave energy to local heat to produce hyperthermia and subsequently destroy tumor cells. Indocyanine green (ICG) is the only clinical agent approved by the U.S. Food and Drug Administration (FDA) for NIR imaging and laser-mediated PTT.[29,30] However, poor spatial resolution, lack of intrinsic tumor targeting specificity, and concentration-dependent aggregation due to poor aqueous stability have limited the effect of ICG on the ablation of malignant tumors.[31,32] Incorporating ICG into nanoparticle (NP) delivery systems may overcome these limitations.[33,34]

Specific target to cancer cells could decrease the toxicity and side effects of therapeutic agents to normal tissues and increase the local dose at the disease lesions. Galactose residues are an attractive targeting ligand for HCC because of their high binding affinity to the asialoglycoprotein receptor (ASGP-r), which is abundantly expressed on the surface of HCC cells; and it has been proved that Galactose even could be efficiently internalized into the cells through receptor-mediated endocytosis when conjugated with other molecules or nanomaterials.[35,36]

In this study, we developed a multifunctional theranostic agent for targeted MRI/CT dual-mode imaging and PTT for HCC. Herein, lactobionic acid (LA, whose structure contains agalactose residue) and gadolinium(III)−1,4,7,10-tetraacetic acid (Gd(III)-DOTA)-modified [polyethylene glycol-2000]−2-distearoyl-*sn*-glycero-3-phosphoethanolamine (PEG-DSPE) (namely, LA-PEG-DSPE and Gd-DOTA-PEG-DSPE), together with hydrogenated soybean phospholipids (HSPC), were self-assembled onto AuNPs@PDA, whose surface was electrostatically preadsorbed with ICG (ICG-AuNPs@PDA), to form a theranostic agent (referred to as LA-LAPNHs) for simultaneous noninvasive MR/CT dual-modal imaging and targeted PTT of HCC. The multiple functions of the prepared LA-LAPNHs are as follows: (1) ICG was utilized as the NIR laser-mediated PTT agent; (2) AuNPs in the core were utilized as the CT contrast element;[37] (3) galactose residues (derived from LA) at the terminus of PEG-DSPE, which specifically recognize the asialoglycoprotein receptors (ASGP-r) that are abundantly present on the surface of HCC cells, endowed the nanohybrids with a specific HCC targeting ability; and (4) the MRI capability resulted from the Gd(III) chelated by DOTA at the terminus of PEG-DSPE. A schematic view of our experimental design is shown in Figure 1.

RESULTS AND DISCUSSION

Synthesis and Characterization of LA-LAPNHs. The method for preparing LA-LAPNHs is illustrated in Figure 1. First, gold nanoparticles (AuNPs) were synthesized according to a previously published method.[38] Transmission electron microscopy (TEM) images showed that the AuNPs could be well-dispersed in an aqueous solution, demonstrating an average diameter of 14 nm (Figure 2a). However, AuNPs are very unstable under physiological conditions and immediately form large aggregates, which results in rapid clearance from the body.[39] Therefore, the particles must undergo further surface modifications for biomedical applications. Dopamine could bind to the surface of gold nanoparticles through the catechols, then spontaneously self-polymerize under alkaline conditions (pH > 7.5) with oxygen as the oxidant.[40−49] In this study, AuNPs were incubated with dopamine (DA) under an oxidative condition (pH 8.5) to induce the formation of the AuNPs@PDA core−shell structure, which could be clearly distinguished in TEM images (Figure 2b), and the thickness of

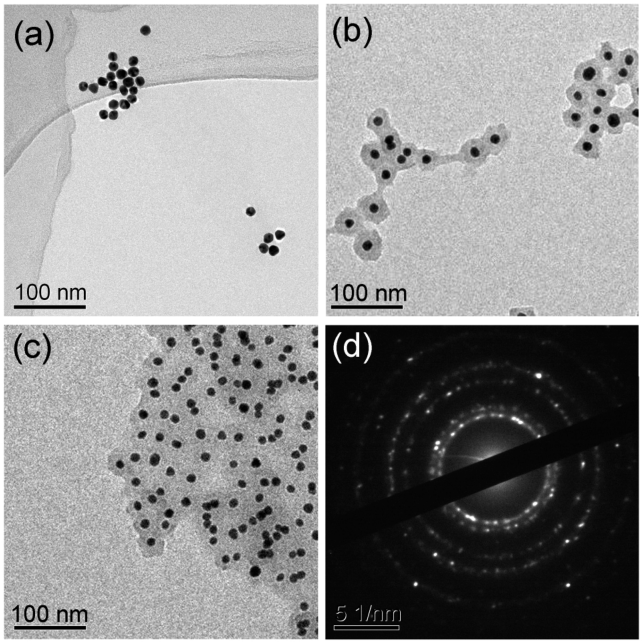

Figure 2. Representative TEM images of (a) AuNPs, (b) AuNPs@PDA, and (C) LA-LAPNHs. (d) The electron diffraction pattern of the LA-LAPNHs. Scale bar: 100 nm for all images.

the PDA coating layer was approximately 7 nm. The visible−near-infrared (vis-NIR) absorbance spectrum of AuNPs@PDA (Figure 3a) in the region of 450−900 nm showed a maximum peak at 520 nm, which was attributed to the distinctive peak of AuNPs. Furthermore, the absorbance of AuNPs@PDA was much higher than that of unmodified AuNPs because of the additional absorbance of the PDA coating layer in this range. To further prove the existence of PDA on the surface of the AuNPs, the Fourier transform infrared (FT-IR) spectra of the obtained product were measured. As shown in Figure 3b, the FT-IR spectra of AuNPs@PDA showed absorption bands at 3410 cm^{-1} (stretching vibration of phenolic O−H and N−H), 1610 cm^{-1} (stretching vibration of aromatic ring and bending vibration of N−H), 1510 cm^{-1} (shearing vibration of N−H), and 1295 cm^{-1} (stretching vibration of phenolic C−O), which supported the presence of PDA on the surface of the AuNPs.

The zeta potential of the obtained AuNPs@PDA was 8.92 ± 1.72 mV in an acidic aqueous solution, which is consistent with the previous report that PDA containing amine (cationic) groups and phenolic hydroxyl (anionic) groups exhibit a negative charge at high pH and a positive charge at low pH.[50,51] The acidic aqueous solution was used as a reaction medium to adsorb negatively charged ICG through electrostatic interactions. After ICG absorption, the zeta potential of the nanohybrid became −2.53 ± 3.52 mV (Figure 3c). It was estimated that 73.5% of the feeding ICG was adsorbed onto the AuNPs@PDA, which was calculated by subtracting the amount of free ICG in the supernatant. In addition, ICG-AuNPs@PDA showed a maximum absorption peak at 785 nm in the NIR region, which was attributed to the distinct absorption peak of ICG (Supporting Information, Figure S1). Strong absorption in the NIR region from 600 to 850 nm is essential for laser-driven photothermal applications.

Next, as the water-soluble AuNPs@PDA tuned to hydrophobic after adsorbing ICG (a hydrophobic molecule), the functionalized Gd-DOTA-PEG-DSPE, LA-PEG-DSPE, and HSPC (at a molar ratio of 3:3:25) could be self-assembled onto the ICG-AuNPs@PDA surface though hydrophobic interaction (the resulting product was referred to as LA-LAPNHs) to induce the capability for HCC-specific targeting and MR imaging. The obtained LA-LAPNHs were stable in phosphate-buffered saline (PBS) solutions for over 30 days, with no apparent aggregates observed (Supporting Information, Figure S2). Good stability is pivotal for the practical applications of the theranostic agent. A typical TEM image of the prepared LA-LAPNHs shows a core−shell morphology (Figure 2c), which is similar to that of AuNPs@PDA (Figure 2b), but with larger aggregates. To verify the chemical composition of the AuNPs@PDA and LA-LAPNHs, energy dispersive spectrometry (EDS) analysis was conducted. As shown in Supporting Information, Figure S3, the elements C, N, O, and Au appeared in the AuNPs@PDA map, while the elements P and Gd appeared in the LA-LAPNHs map in addition to C, N, O, and Au because the Gd-DOTA-modified PEG-DSPE was assembled on AuNPs@PDA. Furthermore, the self-assembly of lipids could be further proved by the FT-IR spectra of the LA-LAPNHs, which show strong lipid CH_2 stretching bands at 2920 and 2848 cm^{-1} compared to the FT-IR spectra of AuNPs@PDA. Several well-defined diffraction rings were observed in the typical selected area electron diffraction (SAED) pattern of the LA-LAPNHs (Figure 2d), which demonstrated that the prepared nanoprobes showed well-defined crystalline features. Dynamic light scattering (DLS) studies showed that the average hydrodynamic sizes of the AuNPs, AuNPs@PDA, ICG-AuNPs@PDA, and LA-LAPNHs were 24.36 ± 6.91 nm, 68.06 ± 9.43 nm, 141.8 ± 8.38 nm, and 220.2 ± 10.32 nm, respectively (Figure 3d). The dramatic increase of the hydrodynamic size after each incorporation step might due to the surface coating induced aggregation; meanwhile, the blackness of the PDA coating also affects the readout of the DLS instrument. The polydispersity index (PDI) of the LA-LAPNHs was 0.143, indicating a relatively uniform size distribution. However, the particle size measured by TEM was smaller than that measured by DLS, most likely due to the nanoparticles under different dry and solution conditions, as well as the small aggregation in solution.[52] After the self-assembly of Gd-DOTA-PEG-DSPE and LA-PEG-DSPE, the zeta potential of the nanocomposite (ζ) switched from −2.53 ± 3.52 mV to 25.1 ± 2.91 mV (Figure 3c). Furthermore, the galactose residues on the surface of the LA-LAPNHs are expected to enable the nanoprobes to specifically target HCC cells via ligand−receptor interactions.

Thermogravimetric analysis (TGA) was used to directly measure the weight loss of the AuNPs and AuNPs@PDA to determine the amount of PDA in the AuNPs@PDA (Supporting Information, Figure S1). Compared with the native AuNPs (approximately 27.5% weight loss), the AuNPs@PDA showed a weight loss of approximately 55.5% from 100 to 600 °C, which means the PDA content should be 28% (Supporting Information, Figure S1). Therefore, the ratio between Au and PDA should be 18:7. However, TGA is not suitable for measuring either the weight loss of ICG in ICG-AuNPs@PDA, because very little amount of ICG was adsorbed, or the weight loss of lipids in LA-LAPNHs due to the incorporation of Gd that could not lose weight from 100 to 600 °C. Therefore, the contents of Au and Gd were determined by inductively coupled plasma−atomic emission spectroscopy (ICP-AES), which were 60.62% and 3% respectively; the content of ICG was determined by measuring the absorbance

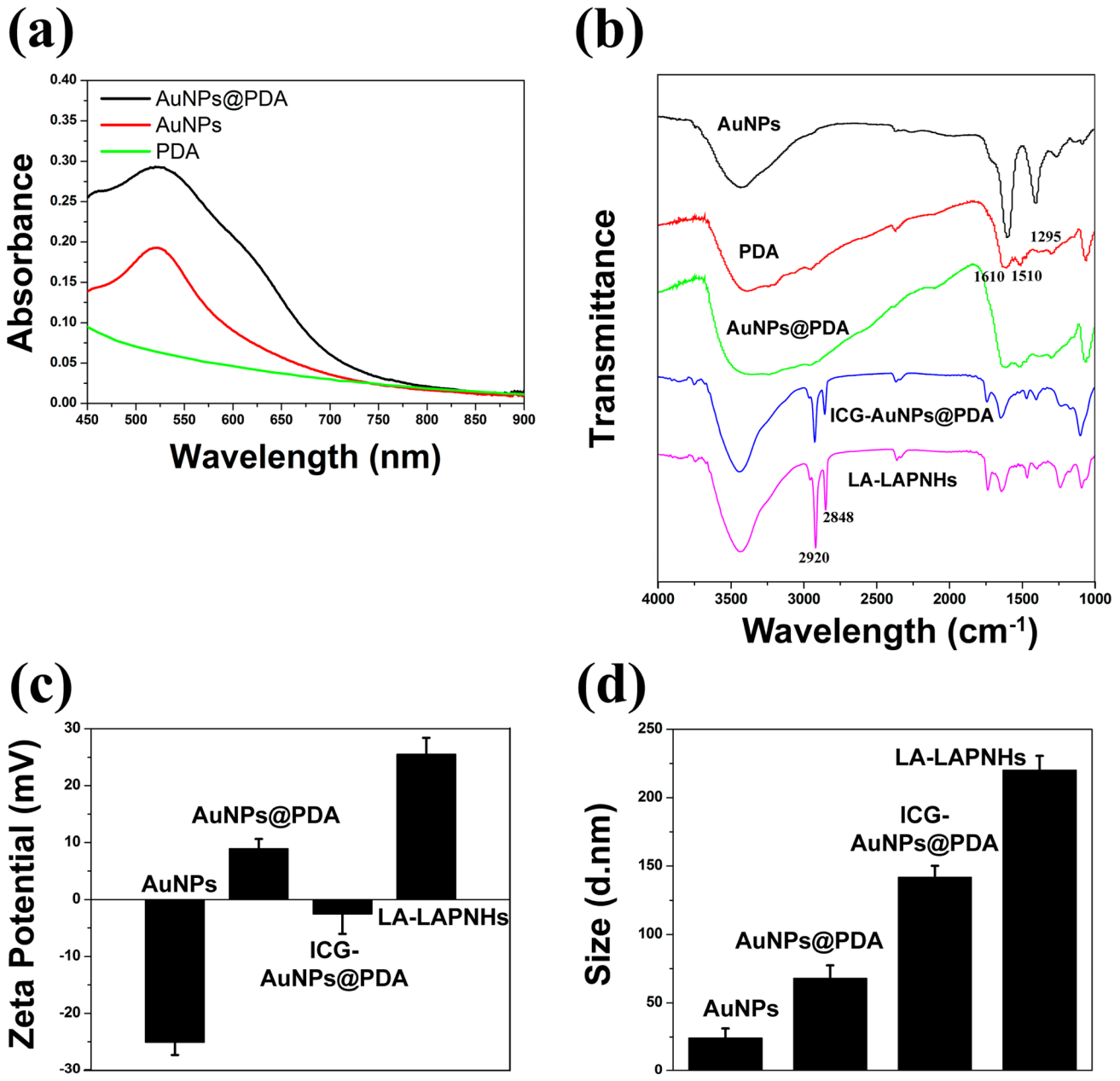

Figure 3. (a) vis–NIR spectra of AuNPs (red), PDA (green), and AuNPs@PDA (black). (b) FT-IR spectra of AuNPs, PDA, AuNPs@PDA, ICG-AuNPs@PDA, and LA-LANPHs. (c) Surface zeta potential of AuNPs, AuNPs@PDA, ICG-AuNPs@PDA, and LA-LAPNHs. (d) Hydrodynamic size of AuNPs, AuNPs@PDA, ICG-AuNPs@PDA, and LA-LAPNHs.

and was 0.62% in LA-LAPNHs. On the basis of the above calculated ratio between Au and PDA, the content of PDA could be calculated to be 23.57%; therefore, the remaining part should be the content of lipids (12.19%).

Confocal Microscopy Studies of the LA-LAPNH Uptake. To examine the characteristics of the LA-LAPNHs as an HCC targeting probe, confocal microscopy imaging was performed. HepG2 cells, an ASGP receptor-positive HCC cell line that could be specifically targeted by LA due to specific recognition between LA and ASGP receptor, were incubated with 0.4 mM of LAPNHs, LA-LAPNHs, and ICG for different durations, whereas HeLa cells without ASGP receptor expression were used as a negative control; since there were no targets available for LA, the LA-LAPNHs would not be specifically internalized. As shown in Figure 4, the red fluorescence from internalized ICG in LA-LAPNH-treated HepG2 cells clearly showed that LA-modified LAPNHs could be effectively internalized into HepG2 cells, and this red fluorescence intensity was much higher than that of LAPNH-treated HepG2 cells after 5 h of incubation. In contrast, following the 5 h incubation period, there was no apparent red fluorescence in HeLa cells treated with the equivalent concentration of LA-LAPNHs, and similar results were obtained for LAPNH-treated cells due to the lack of ASGP-r expression in HeLa cells. However, the free ICG was almost equivalently internalized by both cell types through passive diffusion mechanisms (Figure 4d). These results suggest that the increased amount of LA-LAPNHs was taken up by the HepG2 cells due to ASGP-r-mediated endocytosis.

Furthermore, a competition experiment comparing the uptake efficacy of LA-LAPNHs in the presence and absence of free LA (referred to LA + LA-LAPNHs) was performed to

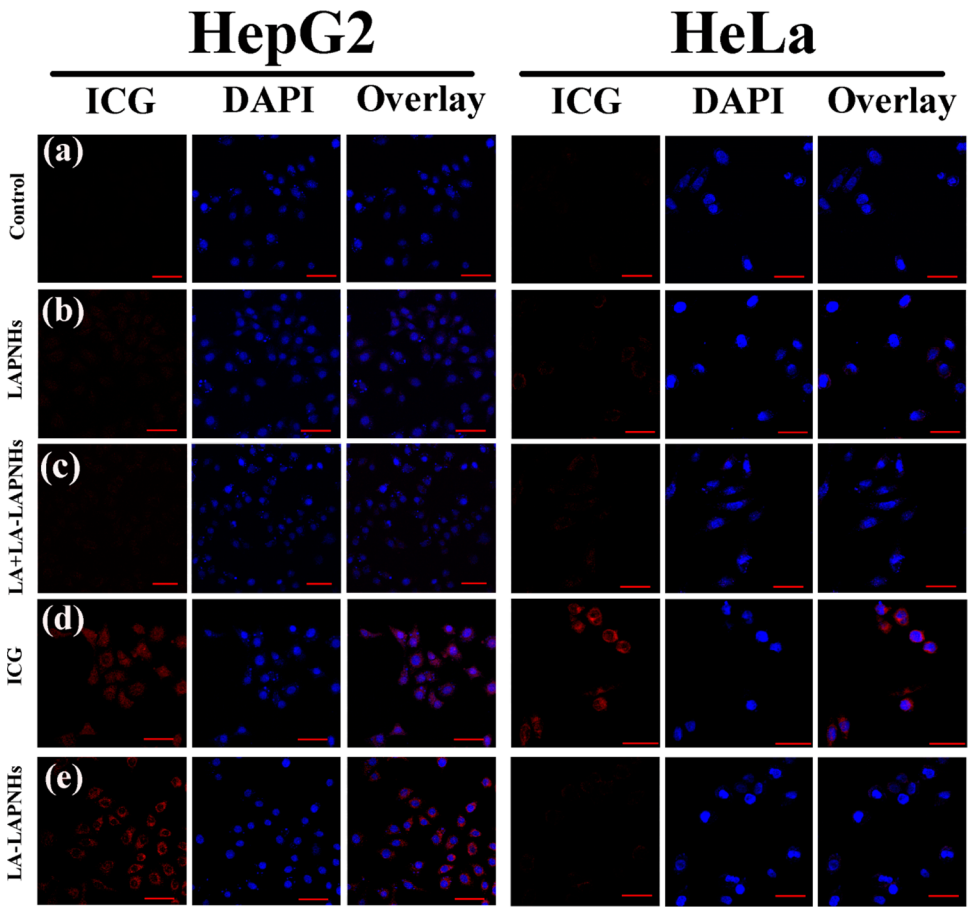

Figure 4. Specific uptake of LA-LAPNHs by the hepatocellular carcinoma cell line HepG2. (a) Control group (cells only); (b) LAPNH-treated group; (c) LA-LAPNH-treated group in the presence of excess free LA; (d) free ICG-treated group; and (e) LA-LAPNH-treated group. Scale bar: 50 μm.

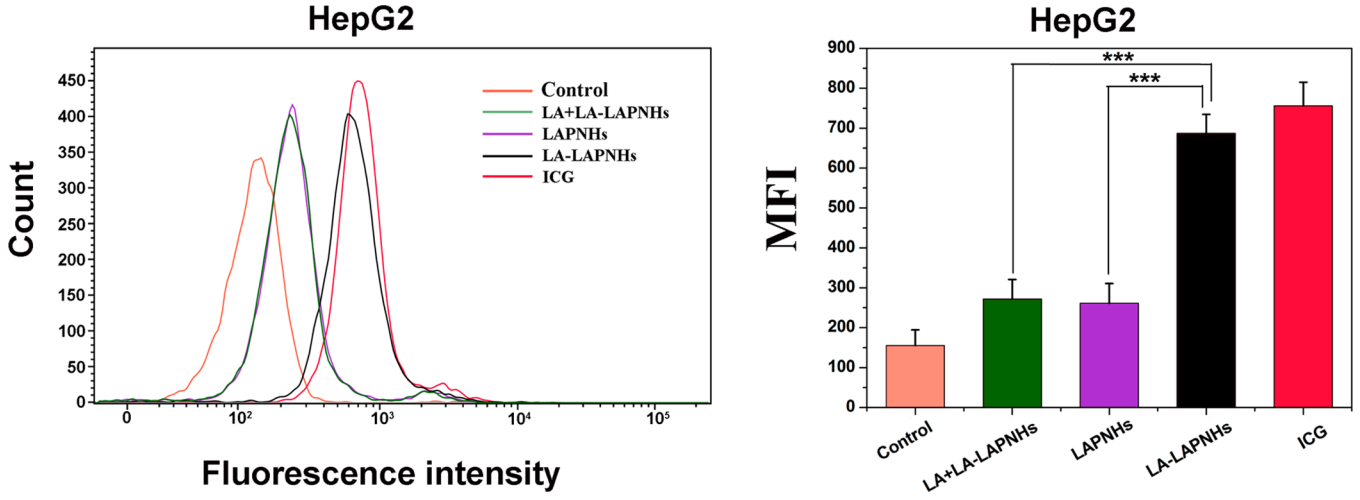

Figure 5. Fluorescence-activated cell sorting (FACS) analysis for HepG2 treated with free ICG, LAPNHs, LA-LAPNHs in the presence or absence of free LA. The representative fluorescence intensity distribution of each group was shown in the left panel. The mean fluorescence intensity (MFI) of each group was shown in the right panel; the experiments were independently repeated three times, and the data was presented by mean ± standard deviation (SD). Statistical analysis was performed with the two-tailed unpaired Student's *t* test, $p < 0.05$ was taken as significantly different, ***$p < 0.001$.

demonstrate that LA-modified nanocomposites engage in specific interactions with HepG2 via the recognition between the ligand (LA) and receptor (ASGP). As shown in Figure 4c, the uptake of LA-LAPNHs was significantly blocked in HepG2 cells due to the presence of excessive free LA, which competes for surface receptor binding. These data suggest that the increased cellular uptake of LA-LAPNHs may be attributed to the specific interaction between the LA moieties and ASGP-r on HepG2 cells.

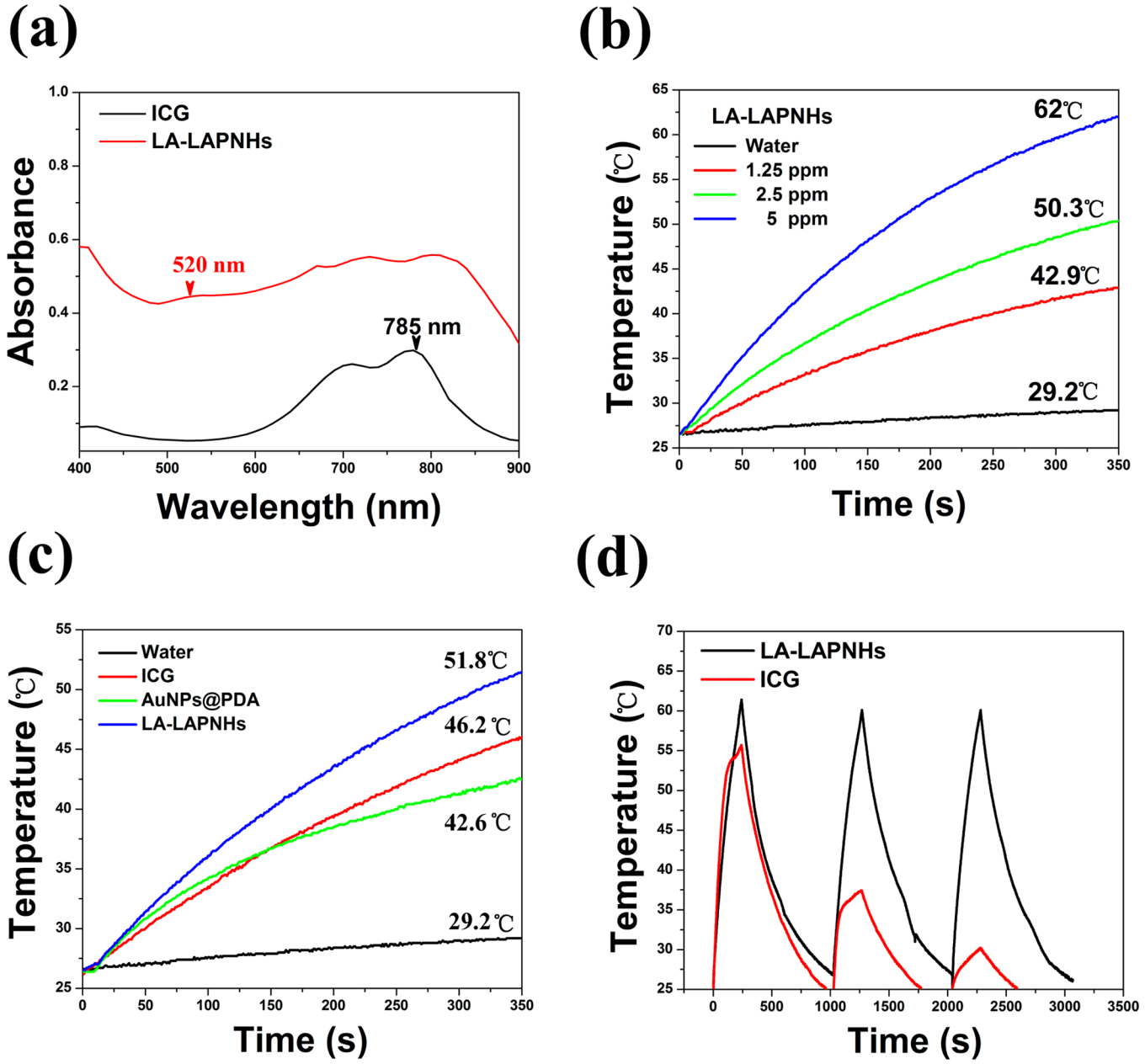

Figure 6. (a) vis-NIR spectra of the prepared LA-LAPNHs and ICG. (b) Temperature elevation curves of LA-LAPNHs at different concentrations. (c) Temperature elevation curves of AuNPs (0.125 mM), free ICG (2.5 μg/mL), and LA-LAPNHs (containing 0.125 mM AuNPs and 2.5 μg/mL ICG). (d) Temperature elevation curves of LA-LAPNHs and free ICG over three rounds of on/off cycling with the 808 nm NIR laser.

Evaluation of Cellular Uptake of LA-LAPNHs by Flow Cytometry. The flow cytometry experiment was carried out to quantitatively study the specific internalization of LA-LAPNHs in HepG2 cells. The cellular uptake efficiency could be indicated by the fluorescence intensities of the cells. As shown in Figure 5, the LAPNHs-treated group had significantly lower internalization of nanoparticles (MFI 280) than the LA-LAPNHs-treated group ($p < 0.01$, MFI 690, which is almost comparable with the free ICG-treated group), because of the specific HCC targeting ability of LA. Meanwhile, the specific internalization of LA-LAPNHs could be blocked in the presence of free LA (LA + LA-LAPNHs, MFI 290, $p < 0.01$) due to their competition. These results were well-consistent with the confocal microscopy results.

Temperature Elevation Induced by NIR Laser Irradiation and Photothermal Stability Study. The vis-NIR absorbance spectrum of LA-LAPNHs shown in Figure 6a indicates strong absorption in the wavelength range of 400–900 nm. The absorption of LA-LAPNHs in the range of 400–650 nm is mostly attributed to AuNPs@PDA. However, the distinct absorption peak of AuNPs at 520 nm was not apparent, which may due to the additive effect of multicomposite absorption in this range. Because the LA-LAPNHs showed strong absorption in the NIR region from 600 to 850 nm with a maximum absorption peak at 785 nm due to ICG incorporation (Figure 6a), the particles may be further used for PTT. As shown in Figure 6b, following exposure to laser irradiation (808 nm, 2 W/cm^2) for 5 min, the temperature of LA-LAPNH dispersions containing 1.25 μg/mL, 2.5 μg/mL, and 5 μg/mL

dx.doi.org/10.1021/am503583s | ACS Appl. Mater. Interfaces 2014, 6, 14266–14277

ICG increased by 16.5, 25.4, and 35.5 °C, respectively. For the 5 μg/mL concentration, the temperature increased to above 60 °C, which is sufficient to kill cancer cells. As the control, the temperature of the deionized water showed no significant changes when exposed to the laser irradiation. As shown in Figure 6c, the temperature elevation of the LA-LAPNHs containing 1.25 μg/mL ICG and 0.125 mM AuNPs@PDA was much higher than that of the same concentration of ICG (1.25 μg/mL) and the same concentration of AuNPs@PDA (0.125 mM) due to the combined photothermal effect of ICG and PDA contained in the LA-LAPNHs.[53] These results suggest that our prepared LA-LAPNHs could act as efficient NIR light absorbers for PTT. In addition, the photothermal stability of the nanoprobe also plays a significant role in PTT during NIR laser irradiation. To investigate the photothermal stability of the LA-LAPNHs under NIR irradiation, the nanoprobes were subjected to three rounds of repeated irradiation using laser on/off cycling in 1000 s intervals. As shown in Figure 6d, the LA-LAPNHs maintained excellent photothermal stability during repeated irradiation without experiencing any decrease in their temperature elevation ability due to the lipid layer of the LA-LAPNHs, which protected the entrapped ICG from being destroyed by the surrounding environment.[54,55] In contrast, the photothermal stability of the free ICG was reducing during repeated irradiation due to the destruction of ICG.

In Vitro Cytotoxicity and Photothermal-Induced Cell Death. Nontoxicity or low toxicity is a key criterion of any nanomaterial designed for biomedical applications. Cell viability assays (CCK-8) were performed to investigate the cytotoxicity of LA-LAPNHs. HepG2 liver cancer cells and HL-7702 normal liver cells were incubated with LA-LAPNHs of gradient concentrations for 24 h. As shown in Figure 7a, in the absence of laser irradiation, these two cell lines treated with LA-LAPNHs remained more than 93% viable at concentrations up to 0.6 mM. These results clearly demonstrated that the LA-LAPNHs did not cause noticeable cell death in either the cancer or noncancer cell line without laser irradiation, which suggests that our nanoprobes exhibit low cytotoxicity. In contrast, cell viability was significantly reduced when the HepG2 cells were exposed to LA-LAPNHs and irradiated with a NIR laser (Figure 7b). At a concentration of 0.6 mM, cell viability was reduced to 13%, which demonstrated the excellent photothermal killing effect of our nanoprobes. To further evaluate the localized tumor photothermal killing effect of LA-LAPNHs, HepG2 cells were incubated with 0.4 mM LA-LAPNHs for 5 h, then irradiated with a NIR laser (808 nm, 2 W/cm^2) for 5 min. Next, the cells were stained with calceinacetoxymethyl ester (calcein AM), which is only incorporated into live cells. As shown in Figure 8d, confocal microscopy revealed that LA-LAPNHs caused marked cell death only via the photothermal cytotoxicity induced by NIR irradiation. Most of the cells outside of the illumination zone showed the green fluorescence of calcein AM, which indicated the survival of HepG2 cells, whereas a small number of cells that were close to the outside edge of the illumination zone also died because of the spread of heat outside of the laser irradiation area. Nevertheless, neither the LA-LAPNHs nor laser irradiation alone induced cell death. These experimental findings demonstrate the significant photothermal therapeutic effect of the LA-LAPNHs and thus clearly suggest that the LA-LAPNHs may act as a potential NIR photoabsorber for the PTT treatment of HCC.

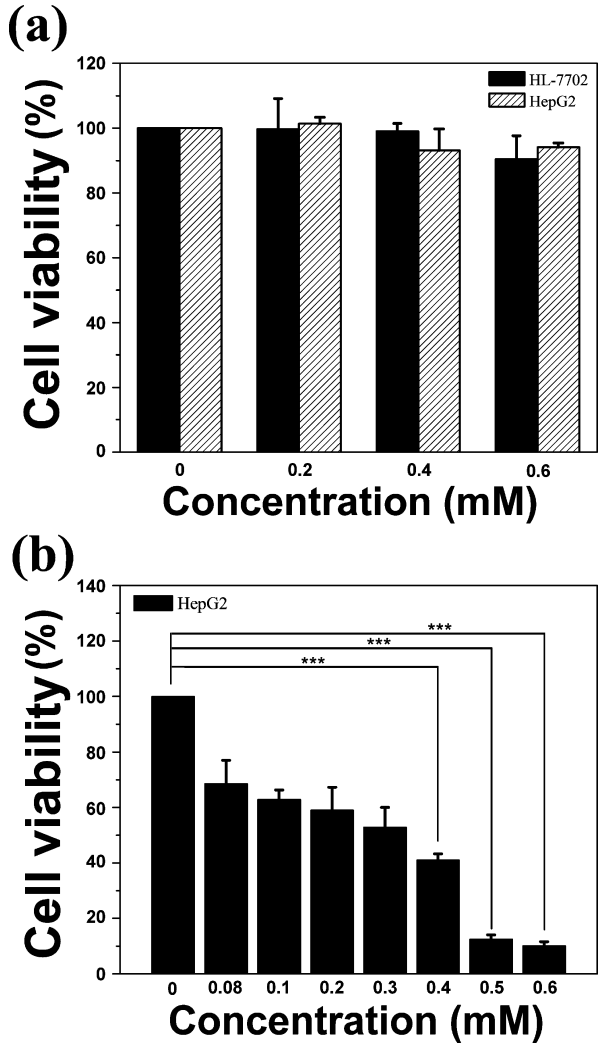

Figure 7. (a) Cell viability of HepG2 and HL-7702 cells treated with different concentrations of LA-LAPNHs without laser irradiation. Bars: mean SD (n = 6). (b) Cell viability of HepG2 cells treated with different concentrations of LA-LAPNHs followed by irradiation with the 808 nm laser (2 W/cm^2, 5 min). Statistical analysis was performed with the two-tailed unpaired Student's t test, $p < 0.05$ was taken as significantly different, *** $p < 0.001$.

In Vitro MRI and CT. To examine the MR imaging function of the LA-LAPNHs, an in vitro T_1-weighted MR imaging experiment was conducted on a 9.4 T (Siemens Magnetom) Trio system.[26] Tubes containing the LA-LAPNH solution were arrayed by increasing concentration, and water was placed as the control. As shown in Figure 9a, positive enhancement of the MRI signal in the LA-LAPNHs was observed compared to water, and the T_1-weighted MR images became brighter, corresponding to the increase in the LA-LAPNH concentration. The T_1 relaxation time for each sample at 20 °C is shown in Table 1, and the results indicate that the LA-LAPNHs shortened the T_1 relaxation time. Further analysis of the observed longitudinal rates revealed a linear dependence on the concentration of dispersed LA-LAPNHs in all measurements (Supporting Information, Figure S5a). The longitudinal coefficient relaxivity value, r_1, which was determined from the slope of the plot of $1/T_1$ versus the sample concentration, was 512.52 mM^{-1} s^{-1}. In contrast, the r_1 value of commercially available injected dimeglumine gadopentetate was only 69.85

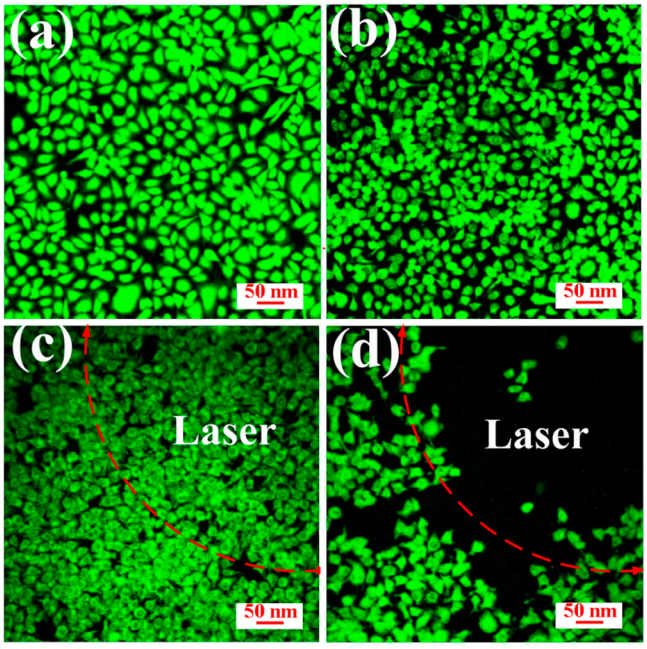

Figure 8. Photothermal destruction of HepG2 cells (a) without LA-LAPNHs or laser irradiation; (b) with LA-LAPNHs but without laser irradiation; (c) with laser irradiation for 5 min but without NPs; and (d) LA-LAPNHs combined with NIR laser irradiation (808 nm, 2 W/cm^2) for 5 min.

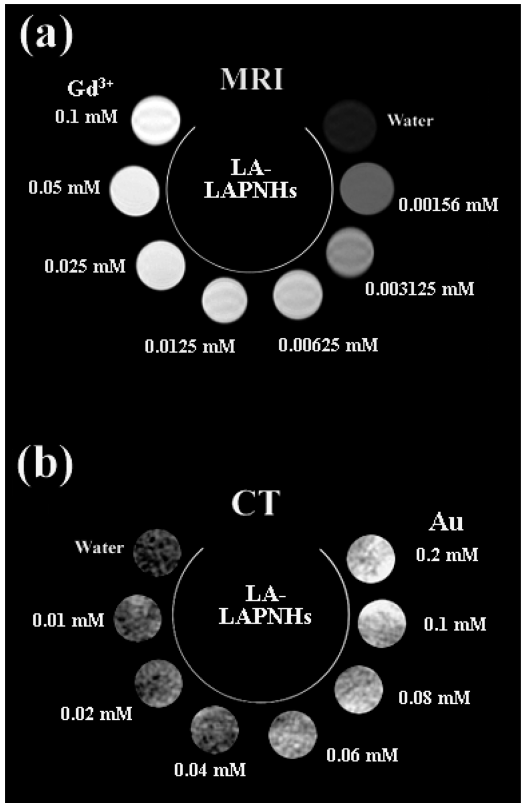

Figure 9. (a) T_1-weighted MR images of LA-LAPNHs at various concentrations. Signal strength is indicated by the brightness of the images. (b) Micro-CT images of LA-LAPNHs of different concentrations. Signal strength is indicated by the brightness of the images.

mM^{-1} s^{-1} (see Table and Supporting Information, Figure S5a). The high molecular relaxivity of LA-LAPNHs may result from both the additive effect of all of the Gd^{3+} paramagnetic centers and the reduction of the molecular tumbling rate, which increases the r_1 value of each Gd-chelate in the confined space of LA-LAPNHs.[56] In addition, because Au exhibits high X-ray attenuation due to its high atomic number and electron density, the CT imaging enhancement ability of LA-LAPNHs was also confirmed by applying a micro-CT imaging system. To determine the feasibility of using LA-LAPNHs as an X-ray CT contrast agent, the X-ray CT images of a phantom were obtained at different concentrations (0.01, 0.02, 0.04 0.06, 0.08, 0.1, and 0.2 mM). As shown in Figure 8b, the brightness of the CT images increased with the LA-LAPNH concentration. Supporting Information, Figure S5b shows that the Hounsfield unit of the LA-LAPNHs increased linearly with concentration (R^2 = 0.998). These results clearly suggest that our LA-LAPNHs have great potential for application in MRI/CT dual-mode imaging.

CONCLUSION

In conclusion, we successfully developed a nanohybrid (LA-LAPNHs) for targeted MRI/CT dual-mode imaging and PTT of HCC. The gold core of LA-LAPNHs could function as a CT imaging contrast agent, and the presence of Gd-DOTA coupled at the terminus of PEG-DSPE could function as an MR imaging contrast-enhancement agent. The prepared LA-LAPNHs could specifically target the HCC cell line HepG2 rather than HeLa cells, due to the specificity of the ligand−receptor recognition between LA and ASGP-receptor, and act as a photothermal therapeutic agent following NIR laser irradiation. Furthermore, the incorporated ICG inside the lipid bilayer has much higher photothermal stability than free ICG, which should further facilitate the clinical usage of our LA-LAPNHs. Therefore, as mentioned above, the prepared LA-LAPNHs may be a promising dual-mode MRI/CT imaging theranostic agent for further treatment and early diagnosis of hepatocellular carcinoma.

EXPERIMENTAL SECTION

Materials. Hydrogen tetrachloroaurate ($HAuCl_4$, CAS: 27988-77-8), *N*-hydroxysuccinimide ester (NHS, CAS: 106627-54-7), and *N*-(3-dimethylaminopropyl)-*N*-ethylcarbodiimide hydrochloride (EDC, CAS: 25952-53-8) were purchased from Sigma-Aldrich. Gadolinium chloride ($GdCl_3$, CAS: 10138-52-0), sodium citrate tribasic dehydrates (CAS: 6132-04-3), hydrogenated soybean phospholipids (HSPC, CAS: 92128-87-5), and lactobionic acid (LA, CAS: 96-82-2) were purchased from J&K Scientific. The compound 2-distearoyl-*sn*-glycero-3-phosphoethanolamine-*N*-[amino(polyethylene glycol)-2000] (H_2N-PEG-DSPE, CAS: 474922-26-4) was purchased from Nanocs. The compounds 1,4,7,10-tetraacetic acid mono-*N*-hydroxysuccinimide ester and B-280 (DOTA-NHS,CAS: 170908-81-3) were purchased from Macrocyclics. Injected dimeglumine gadopentetate (a commercial MRI contrast agent) was purchased from BEILU Pharmaceutical Co., Ltd. (Beijing, PRC). 4′,6-Diamidino-2-phenylindole dihydrochloride (DAPI) (CAS: 28718-90-3) and ICG (CAS: 3599-32-4) were purchased from Dojindo Molecular Technologies. Deionized water with a resistivity of 18.2 MΩ·cm was obtained from a Milli-Q Gradient System (Millipore, Bedford, MA, U.S.) and was used for all experiments. Unless specified, all other chemicals were commercially available and used as received.

Cell Culture. The human HCC cancer cell line HepG2, the normal human hepatocyte cell line HL-7702, and the human cervical cancer cell line HeLa were maintained as monolayer cultures in RPMI-1640 medium supplemented with 10% fetal bovine serum (Atlanta

Table 1. Results of T_1 Time of LA-LAPNH Dispersion at Various Concentrations

sample	H_2O	0.001 5625 mM	0.003 135 mM	0.006 25 mM	0.0125 mM	0.025 mM	0.05 mM	0.1 mM
T_1 time (ms)	2565.70 ± 17.77	596.738 ± 100.54	489.03 ± 105.21	470.233 ± 97.05	462.552 ± 139.76	112.281 ± 34.12	71.358 ± 14.32	20.0772 ± 5.37

Table 2. Results of T_1 Time of Commercial "Injected Dimeglumine Gadopentetate" Dispersion at Various Concentrations

sample	H_2O	0.001 5625 mM	0.003 135 mM	0.006 25 mM	0.0125 mM	0.025 mM	0.05 mM	0.1 mM
T_1 time (ms)	2746.96 ± 18.23	730.131 ± 190.28	672.26 ± 132.47	567.8 ± 79.83	454.15 ± 126.27	331.2 ± 44.32	205.56 ± 19.88	121.195 ± 4.69

Biologicals, Lawrenceville, GA, USA) and 1% penicillin−streptomycin (Gibco BRL, Grand Island, NY, USA) at 37 °C in a humidified atmosphere (5% CO_2).

Synthesis of the LA-LAPNHs. AuNPs were prepared as previously described.[36] Briefly, 1 mL of $HAuCl_4$ (20 mg/mL) was dissolved in deionized water (49 mL) under vigorous stirring at 130 °C, followed by the addition of trisodium citrate solution, causing the color of the mixture to change from blue to burgundy. After it was stirred for another 20 min, the solution was cooled to room temperature and then mixed with 50 mL of DA solution (0.4 mg/mL in 10 mM Tris-HCl, pH 8.5) with slight stirring for 4 h. PDA-coated AuNPs (AuNPs@PDA) were collected by centrifugation at 9000*g* for 15 min and washed three times with deionized water. Next, ICG was adsorbed onto the AuNPs@PDA by the simple mixing of the ICG aqueous solution (20 μg/mL) with 1 mM AuNPs@PDA. The ICG-AuNPs@PDA were collected by centrifugation at 10 000*g* for 15 min and then washed three times with deionized water. The amount of adsorbed ICG was determined by measuring the absorbance at 780 nm.

Next, H_2N-PEG-DSPE (2.1 mM) and DOTA-NHS (4.2 mM) were added to a centrifugation tube and shaken for 12 h at 4 °C. The crude product was dialyzed against deionized water for 48 h molecular weight cut off (MWCO) (MWCO = 3500 Da) to remove free DOTA-NHS. Subsequently, the obtained product was resuspended in water, and its concentration was adjusted to 1 mM; then, an excess volume of $GdCl_3$ aqueous solution (10 mM) was added to the above-mentioned solution, and the mixture was further shaken for 24 h at room temperature. This mixture was then further dialyzed against deionized water for 48 h (MWCO = 3500 Da) to obtain Gd-DOTA-PEG-DSPE. The amount of Gd bound to DOTA-PEG-DSPE was determined through XSERIES 2 inductively coupled plasma mass spectrometry (ICP-MS) (Thermo, USA). To obtain the LA-PEG-DSPE, LA-NHS (10 mM) that was obtained from the activation by EDC/NHS (molar ratio, LA/EDC/NHS = 1:4:2) was added to the 2.1 mM PEG-DSPE aqueous solution. Next, the mixture was shaken for 24 h at 4 °C. The crude product was dialyzed against deionized water for 48 h (MWCO = 3500 Da) to remove excess LA, EDC, and NHS. The obtained product was resuspended in water, and its concentration was adjusted to 1 mM. The presence of galactose residues on LA-PEG-DSPE was determined by the phenol−vitriol method.[37]

Finally, Gd-DOTA-PEG-DSPE, LA-PEG-DSPE, and HSPC were self-assembled on the ICG-AuNPs@PDA as follows: HSPC, Gd-DOTA-PEG-DSPE, and LA-PEG-DSPE were dissolved in 10 mL of $CHCl_3$ in a molar ratio of 25:3:3 and transferred into a round-bottom flask. Then, 10 mL of the ICG-AuNPs@PDA solution (containing 5 μg/mL ICG) was added to the above-mentioned mixture. Next, the $CHCl_3$ in the mixture was evaporated under vigorous stirring for 1 h at 65 °C. Subsequently, the prepared LA-LAPNHs were purified by dialysis (MWCO = 10 kDa) in deionized water for 3 d. To serve as a control, an analogous nanohybrid, but one without the LA modification (referred to LAPNHs), was also prepared and characterized. The synthesis procedure of LAPNHs was similar to that of LA-LAPNHs, but LA-PEG-DSPE was replaced by PEG-DSPE.

Characterization of the LA-LAPNHs. The vis−NIR absorbance of LA-LAPNHs was measured by a vis−NIR spectrometer (Beijing Perkinje General Instrument Co., China). TEM and EDS analyses were performed using a JEM-2010 (JEOL, Japan) electron microscope to characterize the overall morphology and the chemical composition of the samples. Electron diffraction patterns were obtained using a JEM-2100 electron microscope. FT-IR spectra were recorded on a Nicolet 6700 FT-IR spectrometer. The DLS experiments were performed at 25 °C on a NanoZS (Malvern Instruments, Malvern UK) with a detection angle of 173° and a 3 mW He−Ne laser operating at a wavelength of 633 nm. The Z-average particle diameter and the PDI values were obtained by analyzing the correlation functions through cumulants analysis. Zeta potential measurements were performed at 25 °C on the NanoZS, using M3-PALS technology. The Au and Gd content in the LA-LAPNHs and the Gd content in the injected dimeglumine gadopentetate were determined by an ICP-AES system (Thermo Electron, U.S.). TGA was conducted using a diamond DSC/TG/GTA Instruments (PerkinElmer USA) at a heating rate of 10 °C min^{-1} under a nitrogen purge of 40 mL min^{-1} from 50 to 600 °C.

Temperature Elevation Induced by NIR Laser Irradiation. To study the photothermal effect of LA-LAPNHs, 2 mL of aqueous solution with various concentrations of LA-LAPNHs were irradiated by an NIR laser (808 nm, 2 W/cm^2) for 6 min. The temperature of the solutions was monitored by a thermocouple microprobe (Φ = 0.5 mm) (STPC-510P, Xiamen Baidewo Technology Co., China) submerged in the solution every 10 s.

Confocal Microscopy Studies of LA-LAPNHs Uptake. The uptake of LA-LAPNHs and LAPNHs by HepG2 or HeLa cells was investigated using confocal microscopy. HepG2 or HeLa cells (5×10^4) were seeded onto 35 mm glass-bottom Petri dishes and cultured for 24 h at 37 °C in the incubator. Then, the LA-LAPNHs or LAPNHs were added to the cells and incubated for 5 or 24 h. Subsequently, the HepG2 or HeLa cells were washed three times with PBS (pH 7.4) and fixed with 4% paraformaldehyde for 15 min; the nuclei were then stained with 2.0 μM DAPI. Finally, the cells were imaged by confocal microscopy (Nikon A1R-AI Confocal Microscope System) with 633 nm laser excitation for ICG and 405 nm laser excitation for DAPI.

Evaluation of Cellular Uptake of LA-LAPNHs by Flow Cytometry. The nanoparticle uptake capability of the HepG2 and HeLa cell lines was quantitatively analyzed using flow cytometry (BD FACSverse) at an excitation wavelength of 648 nm. In a typical experiment, cells (HepG2 or HeLa) were seeded onto a six-well plate at a density of 2.0×10^5 cells per well in 2 mL of RPMI-1640 medium supplemented with 10% fetal bovine serum (FBS) and cultured for 24 h at 37 °C in a 5% CO_2 atmosphere. The cells were then incubated with LA-LAPNHs or LAPNHs in Dulbecco's modified Eagle's medium (DMEM) at a final ICG concentration of 2.5 μg/mL for 5 h at 37 °C. Next, the culture medium was removed, and cells were washed twice with PBS to remove free particles that had not been uptaken by the cells. Subsequently, the cells were detached from their substrate by incubation with trypsin for 1 min and then were terminated by the addition of complete RPMI-1640 medium containing 10% FBS. Afterward, approximately 4 mL of PBS was added to each well, and the cell suspensions were centrifuged at 1000 rpm for 5 min. After removal of the supernatant, the cells were resuspended in 4 mL of PBS followed once more by centrifugation. Finally, the cells were resuspended in 1 mL of PBS and then filtered through a 40 mm nylon mesh to remove cell aggregates before fluorescence-activated cell sorting (FACS) analysis.

Cytotoxicity Assay and Photothermal-Induced Cell Death. The localized photothermal cell toxicity of LA-LAPNHs was evaluated on HepG2 cells. For qualitative analysis, HepG2 cells (5×10^4) were seeded onto a 35 mm glass-bottom Petri dish and cultured for 24 h at

37 °C in the incubator. The cells were then incubated with LA-LAPNHs for 5 h at 37 °C. Subsequently, the cells were washed three times with PBS to remove free NPs. Then, fresh culture medium was added, and the cells were exposed to NIR laser radiation (2 W/cm^2) for 5 min. After laser irradiation, the cells were washed with PBS and stained with 2.0 μM calcein AM for the visualization of living cells.

To further quantitatively evaluate the cell survival rate after laser irradiation, a Cell Counting Kit-8 (CCK-8) was used to study the photothermal cell toxicity of LA-LAPNHs. In a typical experiment, HepG2 cells were first seeded onto a 96-well plate at a density of 1 × 10^4 cells per well at 37 °C in a 5% CO_2 atmosphere for 24 h. Then, the cell culture medium was discarded, and the cells were washed three times with PBS to remove dead cells, followed by incubation with different concentrations of LA-LAPNHs dispersed in RPMI-1640 medium at 37 °C for 5 h. Next, the cells were washed three times with PBS to remove free NPs. Then, fresh culture medium was added, and the cells were exposed to NIR laser radiation (2 W/cm^2) for 5 min. Following laser irradiation, the cells were incubated with fresh RPMI-1640 culture medium containing 10% fetal bovine serum at 37 °C for 24 h. Then, a CCK-8 was used to measure the cell survival rate according to the manufacturer's protocol. The proliferation of cells was determined by measuring the absorption intensity at 450 nm. Cell viability was expressed as follows: cell viability (%) = $(OD_{sample} - OD_{blank})/(OD_{control} - OD_{blank}) \times 100$. The OD_{sample} and $OD_{control}$ are the absorbance values of the treated cells (as indicated) and the untreated control cells (without both nanoparticles and laser radiation), respectively. The OD_{blank} was the absorbance of CCK8 reagent itself at 450 nm. All experiments were performed in quadruplicate.

In Vitro MRI and CT. Aqueous dispersions of LA-LAPNHs of different concentrations were investigated using T_1/T_2-weighted MRI on a 9.4 T small animal MRI scanner (Bruker Avance II 500 WB spectrometer) to evaluate the contrast-enhancement effect. T_1/T_2-weighted imaging was performed using an inversion recovery gradient echo sequence with TE = 4 ms, a slice thickness of 0.5 mm, an field of view (FOV) of 3.0 × 3.0 cm, and a matrix size of 128 × 128. Injected dimeglumine gadopentetate (a commercial MRI contrast agent) was used as a control.

CT scans were performed using a GE Light Speed VCT imaging system (GE Medical Systems) operated at 100 kV and 80 mA, with a slice thickness of 0.625 mm. Solutions of LA-LAPNHs (0.2 mL) with different Au concentrations were prepared in 2.0 mL Eppendorf tubes and placed in a self-designed scanning holder. Contrast enhancement was determined in Hounsfield units for each sample.

■ ASSOCIATED CONTENT

Supporting Information

Additional vis−NIR spectroscopy data, the photograph of LA-LAPNHs, the energy dispersive spectrometry, the thermal decomposition curve, the proton T_1 relaxation rate, and Hounsfield units plot of LA-LAPNHs. This material is available free of charge via the Internet at http://pubs.acs.org.

■ AUTHOR INFORMATION

Corresponding Author

*E-mail: xiaoloong.liu@gmail.com.

Notes

The authors declare no competing financial interest.

■ ACKNOWLEDGMENTS

This work is supported by the National Natural Science Foundation of China (Grant No. 31201008), the University Natural Science Foundation of Jiangsu Province (Grant No. 12KJB180013), the research development foundation of Fujian Medical University (Grant No.FZS13001Y), and the Backbone Talents Training Project of Fujian Health Department (Grant No. 2013-ZQN-ZD-29).

■ REFERENCES

(1) Bosch, F. X.; Ribes, J.; Diaz, M.; Cleries, R. Primary Liver Cancer: Worldwide Incidence and Trends. *Gastroenterology* **2004**, *127*, 5−16.
(2) Tang, Y. H.; Wen, T. F.; Chen, X. Anatomic Versus Non-anatomic Liver Resection for Hepatocellular Carcinoma: A Systematic Review. *Hepato-Gastroenterology* **2013**, *60*, 2019−2025.
(3) Abdel-Wahab, M.; Sultan, A. M.; Fathy, O. M.; Salah, T.; Elshobary, M. M.; Elghawalby, N. A.; Yassen, A. M.; Elsarraf, W. M.; Elsaadany, M. F.; Zalatah, K. Factors Affecting Recurrence and Survival after Living Donor Liver Transplantation for Hepatocellular Carcinoma. *Hepato-Gastroenterology* **2012**, *60*, 1847−1853.
(4) Imamura, H.; Kawasaki, S.; Miyagawa, S.; Ikegami, T.; Kitamura, H.; Shimada, R. Aggressive Surgical Approach to Recurrent Tumors after Hepatectomy for Metastatic Spread of Colorectal Cancer to The Liver. *Surgery* **2000**, *127*, 528−535.
(5) Lai, Q.; Nudo, F.; Mennini, G.; Spoletini, G.; Morabito, V.; Levi, S. G.; Melandro, F.; Guglielmo, N.; Berloco, P. B.; Rossi, M. Expanded Criteria for Hepatocellular Carcinoma after Liver Transplantation: A 20-Year Evolution. *Hepato-Gastroenterology* **2013**, *60*, 2039−2041.
(6) Llovet, J. M.; Fuster, J.; Bruix, J. The Barcelona Approach: Diagnosis, Staging, and Treatment of Hepatocellular Carcinoma. *Liver Transpl.* **2004**, *10*, 115−120.
(7) Robinson, P. Hepatocellular Carcinoma: Development and Early Detection. *Cancer Imaging* **2008**, *8*, 128−131.
(8) Li, Y.; Chen, Z.; Li, F.; Wang, J.; Zhang, Z. Preparation and in Vitro Studies of MRI-Specific Superparamagnetic Iron Oxide antiGPC3 Probe for Hepatocellular Carcinoma. *Int. J. Nanomed.* **2011**, *7*, 4593−4611.
(9) Taouli, B.; Johnson, R. S.; Hajdu, C. H.; Oei, M. T.; Merad, M.; Yee, H.; Rusinek, H. Hepatocellular Carcinoma: Perfusion Quantification with Dynamic Contrast-enhanced MRI. *Am. J. Roentgenol.* **2013**, *201*, 795−800.
(10) Sato, T.; Tateishi, R.; Yoshida, H.; Ohki, T.; Masuzaki, R.; Imamura, J.; Goto, T.; Kanai, F.; Obi, S.; Kato, N.; Shiina, S.; Kawabe, T.; Omata, M. Ultrasound Surveillance for Early Detection of Hepatocellular Carcinoma among Patients with Chronic Hepatitis C. *Hepatol. Int.* **2009**, *3*, 544−550.
(11) Salem, N.; Kuang, Y.; Wang, F.; Maclennan, G. T.; Lee, Z. PET Imaging of Hepatocellular Carcinoma with 2-deoxy-2[^{18}F] Fluoro-D-Glucose, 6-Deoxy-6[^{18}F] Fluoro-D-Glucose, [1-^{11}C]-Acetate and [N-methyl-^{11}C]-Choline. *Q. J. Nucl. Med. Mol. Imaging* **2009**, *53*, 144−156.
(12) Cheng, M. F.; Wu, Y. W.; Tzen, K. Y.; Huang, Y. H.; Yen, R. F. Whole-Body F-18 FDG PET for Hepatocellular Carcinoma Patients after Interventional Treatment. *Neoplasma* **2007**, *54*, 342−347.
(13) Kelly, J.; Raptopoulos, V.; Davidoff, A.; Waite, R.; Norton, P. TheValue of Non-Contrast-Enhanced CT in Blunt Abdominal Trauma. *Am. J. Roentgenol.* **1989**, *152*, 41−48.
(14) Hallouard, F.; Anton, N.; Choquet, P.; Constantinesco, A.; Vandamme, T. Iodinated Blood Pool Contrast Media for Preclinical X-ray Imaging Applications Review. *Biomaterials* **2010**, *31*, 6249−6268.
(15) Kattapuram, T. M.; Treat, M. E.; Kattapuram, S. V. Magnetic Resonance Imaging of Bone and Soft Tissue Infections. *Curr. Clin. Top. Infect. Dis.* **2001**, *21*, 190−226.
(16) McCarthy, J. R. Multifunctional Agents for Concurrent Imaging and Therapy in Cardiovascular Disease. *Adv. Drug Delivery Rev.* **2010**, *62*, 1023−1030.
(17) Kelkar, S. S.; Reineke, T. M. Theranostics: Combining Imaging and Therapy. *Bioconjugate Chem.* **2011**, *22*, 1879−1903.
(18) Alric, C.; Taleb, J.; Duc, G. L.; Mandon, C.; Billotey, C.; Meur-Herland, A. L.; Brochard, T.; Vocanson, F.; Janier, M.; Perriat, P. Gadolinium Chelate coated Gold Nanoparticles as Contrast Agents for Both X-ray Computed Tomography and Magnetic Resonance Imaging. *J. Am. Chem. Soc.* **2008**, *130*, 5908−5915.
(19) Narayanan, S.; Sathy, B. N.; Mony, U.; Koyakutty, M.; Nair, S. V.; Menon, D. Biocompatible Magnetite/Gold Nanohybrid Contrast Agents via Green Chemistry for MRI and CT Bioimaging. *ACS Appl. Mater. Interfaces* **2011**, *4*, 251−260.

(20) Sarin, H.; Kanevsky, A. S.; Wu, H.; Brimacombe, K. R.; Fung, S. H.; Sousa, A. A.; Auh, S.; Wilson, C. M.; Sharma, K.; Aronova, M. A. Effective Transvascular Delivery of Nanoparticles across the Blood-Brain Tumor Barrier into Malignant Glioma Cells. *J. Transl. Med.* **2008**, *6*, 80.
(21) Wang, X.; Liu, H.; Chen, D.; Meng, X.; Liu, T.; Fu, C.; Hao, N.; Zhang, Y.; Wu, X.; Ren, J.; Tang, F. Multifunctional Fe_3O_4@P(St/MAA)@Chitosan@AuCore/Shell Nanoparticles for Dual Imaging and Photo-Thermal Therapy. *ACS Appl. Mater. Interfaces* **2013**, *5*, 4966–4971.
(22) Cheung, E. N. M.; Alvares, R. D.; Oakden, W.; Chaudhary, R.; Hill, M. L.; Pichaandi, J.; Mo, G. C.; Yip, C.; Macdonald, P. M.; Stanisz, G. J. Polymer-Stabilized Lanthanide Fluoride Nanoparticle Aggregates as Contrast Agents for Magnetic Resonance Imaging and Computed Tomography. *Chem. Mater.* **2010**, *22*, 4728–4739.
(23) Lee, N.; Cho, H. R.; Oh, M. H.; Lee, S. H.; Kim, K.; Kim, B. H.; Shin, K.; Ahn, T.-Y.; Choi, J. W.; Kim, Y.-W. Multifunctional Fe_3O_4/T_aO_x Core/Shell Nanoparticles for Simultaneous Magnetic Resonance Imaging and X-ray Computed Tomography. *J. Am. Chem. Soc.* **2012**, *134*, 10309–10312.
(24) Huang, Y.; He, S.; Cao, W.; Cai, K.; Liang, X. J. Biomedical Nanomaterials for Imaging-Guided Cancer Therapy. *Nanoscale* **2012**, *4*, 6135–6149.
(25) Ohulchanskyy, T. Y.; Kopwitthaya, A.; Jeon, M.; Guo, M.; Law, W. C.; Furlani, E. P.; Kim, C.; Prasad, P. N. Phospholipid Micelle-Based Magneto-Plasmonic Nanoformulation for Magnetic Field-Directed, Imaging-guided Photo-Induced Cancer Therapy. *Nanomedicine* **2013**, *9*, 1192–1202.
(26) Huang, P.; Lin, J.; Wang, S.; Zhou, Z.; Li, Z.; Wang, Z.; Zhang, C.; Yue, X.; Niu, G.; Yang, M.; Cui, D.; Chen, X. Photosensitizer-Conjugated Silica-Coated Gold Nanoclusters for Fluorescence Imaging-guided Photodynamic Therapy. *Biomaterials* **2013**, *34*, 4643–4654.
(27) Guo, M.; Mao, H.; Li, Y.; Zhu, A.; He, H.; Yang, H.; Wang, Y.; Tian, X.; Ge, C.; Peng, Q.; Wang, X.; Yang, X.; Chen, X.; Liu, G.; Chen, H. Dual Imaging-Guided Photothermal/Photodynamic Therapy using Micelles. *Biomaterials* **2013**, *35*, 4656–4666.
(28) Li, Z.; Zeng, Y.; Zhang, D.; Wu, M.; Wu, L.; Huang, A.; Yang, H.; Liu, X.; Liu, J. Glypican-3 antibody Functionalized Prussian Blue Nanoparticles for Targeted MR Imaging and Photothermal Therapy of Hepatocellular Carcinoma. *J. Mater. Chem. B* **2014**, DOI: 10.1039/C4TB00516C.
(29) Schaafsma, B. E.; Mieog, J. S.; Hutteman, M.; van der Vorst, J. R.; Kuppen, P. J.; Lowik, C. W.; Frangioni, J. V.; van de Velde, C. J.; Vahrmeijer, A. L. The Clinical use of Indocyanine Green as a Near-infrared Fluorescent Contrast Agent for Image-Guided Oncologic Surgery. *J. Surg. Oncol.* **2011**, *104*, 323–332.
(30) Holzer, W.; Mauerer, M.; Penzkofer, A.; Szeimies, R. M.; Abels, C.; Landthaler, M.; Baumler, W. Photostability and Thermal Stability of Indocyanine Green. *J. Photochem. Photobiol., B* **1998**, *47*, 155–164.
(31) Landsman, M. L.; Kwant, G.; Mook, G. A.; Zijlstra, W. G. Light-Absorbing Properties, Stability, and Spectral Stabilization of Indocyanine Green. *J. Appl. Physiol.* **1976**, *40*, 575–583.
(32) Tripp, M. R.; Cohen, G. M.; Gerasch, D. A.; Fox, I. J. Effect of Protein and Electrolyte on the Spectral Stabilization of Concentrated Solutions of Indocyanine Green. *Proc. Soc. Exp. Biol. Med.* **1973**, *143*, 879–883.
(33) Zheng, C.; Zheng, M.; Gong, P.; Jia, D.; Zhang, P.; Shi, B.; Sheng, Z.; Ma, Y.; Cai, L. Indocyanine Green-Loaded Biodegradable Tumor Targeting Nanoprobes for in Vitro and in Vivo Imaging. *Biomaterials* **2012**, *33*, 5603–5609.
(34) Saxena, V.; Sadoqi, M.; Shao, J. Enhanced Photo-stability, Thermal-stability and Aqueous-stability of Indocyanine Green in Polymeric Nanoparticulate Systems. *J. Photochem. Photobiol., B* **2004**, *74*, 29–38.
(35) Liu, H.; Wang, H.; Xu, Y.; Guo, R.; Wen, S.; Huang, Y.; Liu, W.; Shen, M.; Zhao, J.; Zhang, G.; Shi, X. Lactobionic Acid-Modified Dendrimer-Entrapped Gold Nanoparticles for Targeted Computed Tomography Imaging of Human Hepatocellular Carcinoma. *ACS Appl. Mater. Interfaces* **2014**, *6*, 6944–6953.
(36) Zhang, M.; Zhou, X.; Wang, B.; Yung, B. C.; Lee, L. J.; Ghoshal, K.; Lee, R. J. Lactosylated Gramicidin-Based Lipid Nanoparticles (Lac-GLN) for Targeted Delivery of Anti-miR-155 to Hepatocellular Carcinoma. *J. Controlled Release* **2013**, *168*, 251–261.
(37) Hainfeld, J. F.; Dilmanian, F. A.; Slatkin, D. N.; Smilowitz, H. M. Radiotherapy Enhancement with Gold Nanoparticles. *J. Pharm. Pharmacol.* **2008**, *60*, 977–985.
(38) Sugunan, A.; Thanachayanont, C.; Dutta, J.; Hilborn, J. Heavy-Metal Ion Sensors Using Chitosan-Capped Gold Nanoparticles. *Sci. Technol. Adv. Mater.* **2005**, *6*, 335–340.
(39) Wang, Z.; Luo, D.; Ena, C. Optimization of Polysaccharides Extraction from *Gynostemma Pentaphyllum Makino* using Uniform Design. *Carbohydr. Polym.* **2007**, *69*, 311–317.
(40) Tsai, W. B.; Chen, W. T.; Chien, H. W.; Kuo, W. H.; Wang, M. J. Poly (dopamine) Coating of Scaffolds for Articular Cartilage Tissue Engineering. *Acta Biomater.* **2011**, *7*, 4187–4194.
(41) Kim, H. W.; McCloskey, B. D.; Choi, T. H.; Lee, C.; Kim, M. J.; Freeman, B. D.; Park, H. B. Oxygen Concentration Control of Dopamine-Induced High Uniformity Surface Coating Chemistry. *ACS Appl. Mater. Interfaces* **2013**, *5*, 233–238.
(42) Wang, W.; Li, R.; Tian, M.; Liu, L.; Zou, H.; Zhao, X.; Zhang, L. Surface Silverized Meta-Aramid Fibers Prepared by Bio-Inspired Poly(dopamine) Functionalization. *ACS Appl. Mater. Interfaces* **2013**, *5*, 2062–2069.
(43) Liu, R.; Guo, Y.; Odusote, G.; Qu, F.; Priestley, R. D. Core-Shell Fe_3O_4 Polydopamine Nanoparticles Serve Multipurpose as Drug Carrier, Catalyst Support and Carbon Adsorbent. *ACS Appl. Mater. Interfaces* **2013**, *5*, 9167–9171.
(44) Ryu, J.; Ku, S. H.; Lee, H.; Park, C. B. Mussel-Inspired Polydopamine Coating as A Universal Route to Hydroxyapatite Crystallization. *Adv. Funct. Mater.* **2010**, *20*, 2132–2139.
(45) Liu, Y.; Ai, K.; Lu, L. Polydopamine and Its Derivative Materials: Synthesis and Promising Applications in Energy, Environmental, and Biomedical Fields. *Chem. Rev.* **2014**, *114*, 5057–5115.
(46) Liu, X.; Cao, J.; Li, H.; Li, J.; Jin, Q.; Ren, K.; Ji, J. Mussel-Inspired Polydopamine: A Biocompatible and Ultrastable Coating for Nanoparticles in Vivo. *ACS Nano* **2013**, *7* (10), 9384–9395.
(47) Lin, L. S.; Cong, Z. X.; Cao, J. B.; Ke, K. M.; Peng, Q. L.; Gao, J.; Yang, H. H.; Liu, G.; Chen, X. Multifunctional Fe_3O_4@Polydopamine Core–Shell Nanocomposites for Intracellular mRNA Detection and Imaging-Guided Photothermal Therapy. *ACS Nano* **2014**, *8*, 3876–3883.
(48) Park, J.; Brust, T. F.; Lee, H. J.; Lee, S. C.; Watts, V. J.; Yeo, Y. Polydopamine-Based Simple and Versatile Surface Modification of Polymeric Nano Drug Carriers. *ACS Nano* **2014**, *8*, 3347–3356.
(49) Liu, Q.; Wang, N.; Caro, J.; Huang, A. Bio-Inspired Polydopamine: A Versatile and Powerful Platform for Covalent Synthesis of Molecular Sieve Membranes. *J. Am. Chem. Soc.* **2013**, *135*, 17679–17682.
(50) Yu, B.; Liu, J.; Liu, S.; Zhou, F. Pdop Layer Exhibiting Zwitterionicity: A Simple Electrochemical Interface for Governing Ion Permeability. *Chem. Commun.* **2010**, *46*, 5900–5902.
(51) Liu, Q.; Yu, B.; Ye, W.; Zhou, F. Highly Selective Uptake and Release of Charged Molecules by pH-Responsive Polydopamine Microcapsules. *Macromol. Biosci.* **2011**, *11*, 1227–1234.
(52) She, W. C.; Luo, K.; Zhang, C. Y.; Wang, G.; Geng, Y. Y.; Li, L.; He, B.; GuZ, W. The Potential of Self-Assembled, pH-Responsive Nanoparticles of mPEGylated Peptide Dendron-Doxorubicin Conjugates for Cancer Therapy. *Biomaterials* **2013**, *34*, 1613–1623.
(53) Liu, Y. L.; Ai, K. L.; Liu, J. H.; Mo, D.; Yang, H. Y.; Lu, L. h. Dopamine-Melanin Colloidal Nanospheres: an Efficient Near-Infrared Photothermal Therapeutic Agent for in Vivo Cancer Therapy. *Adv. Mater.* **2013**, *25*, 1353–1359.
(54) Zheng, C.; Zheng, M.; Gong, P.; Jia, D.; Zhang, P.; Shi, B.; Sheng, Z.; Ma, Y.; Cai, L. Indocyanine Green-Loaded Biodegradable Tumor Targeting Nanoprobes for in Vitro and in Vivo Imaging. *Biomaterials* **2012**, *33*, 5603–5609.

(55) Saxena, V.; Sadoqi, M.; Shao, J. Enhanced Photo-Stability, Thermal-Stability and Aqueous-Stability of Indocyanine Green in Polymeric Nanoparticulate Systems. *J. Photochem. Photobiol., B* **2004**, *74*, 29−38.
(56) Mi, P.; Kokuryo, D.; Cabral, H.; Kumagai, M.; Nomoto, T.; Aoki, I.; Terada, Y.; Kishimura, A.; Nishiyama, N.; Kataoka, K. Hydrothermally Synthesized PEGylated Calcium Phosphate Nanoparticles Incorporating Gd-DTPA for Contrast Enhanced MRI Diagnosis of Solid Tumors. *J. Controlled Release* **2014**, *174*, 63−71.